LETTER

VIPER: an industrially scalable high-current high-temperature superconductor cable

To cite this article: Zachary S Hartwig *et al* 2020 *Supercond. Sci. Technol.* **33** 11LT01

View the article online for updates and enhancements.

You may also like

Letter

VIPER: an industrially scalable high-current high-temperature superconductor cable

Zachary S Hartwig[1], **Rui F Vieira**[1], **Brandon N Sorbom**[2], **Rodney A Badcock**[4],
Marta Bajko[3], **William K Beck**[1], **Bernardo Castaldo**[3], **Christopher L Craighill**[2],
Michael Davies[4], **Jose Estrada**[1], **Vincent Fry**[1], **Theodore Golfinopoulos**[1],
Amanda E Hubbard[1], **James H Irby**[1], **Sergey Kuznetsov**[2], **Christopher J Lammi**[2],
Philip C Michael[1], **Theodore Mouratidis**[1], **Richard A Murray**[1], **Andrew T Pfeiffer**[1],
Samuel Z Pierson[1], **Alexi Radovinsky**[1], **Michael D Rowell**[1], **Erica E Salazar**[1],
Michael Segal[2], **Peter W Stahle**[1], **Makoto Takayasu**[1], **Thomas L Toland**[1]
and Lihua Zhou[1]

[1] MIT Plasma Science and Fusion Center, 167 Albany St, Cambridge, MA 02139, United States of America
[2] Commonwealth Fusion Systems, 501 Massachusetts Ave, Cambridge, MA 02139, United States of America
[3] CERN, CH-1211 Geneva 23, Geneva, Switzerland
[4] Robinson Research Institute, Victory University of Wellington, 69 Gracefield Rd, Lower Hutt 5046, New Zealand

E-mail: hartwig@psfc.mit.edu

Abstract
High-temperature superconductors (HTS) promise to revolutionize high-power applications like wind generators, DC power cables, particle accelerators, and fusion energy devices. A practical HTS cable must not degrade under severe mechanical, electrical, and thermal conditions; have simple, low-resistance, and manufacturable electrical joints; high thermal stability; and rapid detection of thermal runaway quench events. We have designed and experimentally qualified a vacuum pressure impregnated, insulated, partially transposed, extruded, and roll-formed (VIPER) cable that simultaneously satisfies all of these requirements for the first time. VIPER cable critical currents are stable over thousands of mechanical cycles at extreme electromechanical force levels, multiple cryogenic thermal cycles, and dozens of quench-like transient events. Electrical joints between VIPER cables are simple, robust, and demountable. Two independent, integrated fiber-optic quench detectors outperform standard quench detection approaches. VIPER cable represents a key milestone in next-step energy generation and transmission technologies and in the maturity of HTS as a technology.

Keywords: HTS, superconducting cables, superconducting magnets, quench detection

(Some figures may appear in color only in the online journal)

1. Introduction

Discovered in 1911 [1] and made practical in the 1960s [2], low temperature superconductors (LTS) like NbTi and Nb_3Sn have seen select deployment in accelerator magnets, specialized research instruments, and medical MRIs. Broader application has been limited by cost, material properties, and the engineering and operational challenges of liquid-helium (4 K) temperatures. However, the discovery of ceramic-based superconductors operating above liquid nitrogen (77 K) temperatures in 1987 [3], coupled to present industrial-scale thin-film deposition processes [4, 5], has enabled the production of 100s of km per year of rare earth barium copper oxide (REBCO) high-temperature superconductors (HTS), which alleviate many LTS limitations.

Small bore HTS research magnets have been wound from single tapes [6, 7], while larger-scale applications—accelerator and fusion magnets, generators and motors—must combine many HTS tapes into conductors, or cables, to maximize current capacity, allow sufficient cooling, and provide structural support. There are three principal HTS cable architectures: twisted stack tape conductor (TSTC) [8], conductor on round core (CORC) [9], and Roebel [10]. Despite significant progress [11–17] including a recent successful demonstration of a 4 kA CORC cable in small solenoid coil at 16.5 T [18], no instantiation of these architectures has simultaneously satisfied the challenging requirements of high-field (>15 T) magnets and high-current (>25 kA) applications: (1) stability against critical current degradation under mechanical and thermal cycling; (2) high cryostability and reliable quench detection techniques; and (3) simple, low resistance, and manufacturable electrical joints.

This paper presents the design, fabrication, and qualification of a TSTC-based HTS cable called VIPER that satisfies each of these criteria, resulting in a manufacturable and scalable conductor. VIPER cable length, cross section, shape, and current capacity can be adapted for a variety of high-current applications; here, we primarily focus on a version for high-field DC fusion magnets. Such magnets present some of the most extreme challenges of any superconducting application and, therefore, are a valuable proving ground. By enabling high-field magnetic fusion energy [19], VIPER cables can accelerate the reduction in HTS cost through industry scale up [20] and open new opportunities for HTS technology to impact superconducting magnets, DC transmission lines, generators, and transformers [21].

2. Cable design

VIPER cable comprises a central leak-tight channel carrying cryogenic coolant in a copper core with rectangular channels on the perimeter supporting HTS stacks. The core is fabricated with a continuous extrusion method that is inexpensive, consistent, and scalable to hundreds of meters with tight tolerances. The extrusion and HTS stacks are twisted to (1) eliminate strain accumulation in the HTS during fabrication,
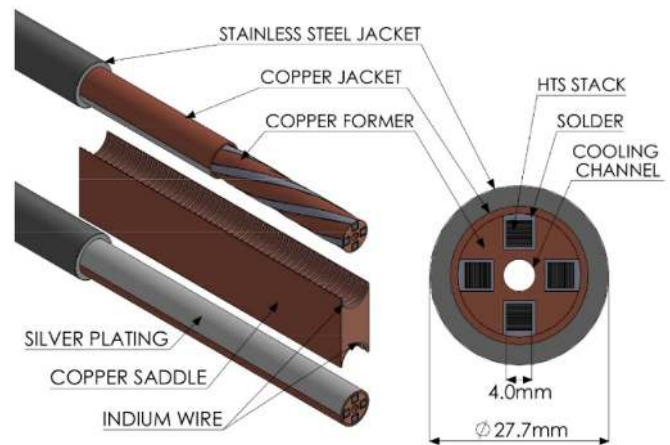

Figure 1. VIPER cables for high-field superconducting fusion magnets. (Right) HTS stacks are VPI soldered into channels in a twisted copper former containing a central cooling channel and surrounded by roll-formed copper and optional stainless-steel jacket. (Left) A cut-away showing that joints are easily created by silver plating the cable ends and compressing them into a copper saddle. Indium wire ensures maximum surface contact for minimal electrical resistance. The joint shown is configured for the SULTAN facility; joints in applications would use a much smaller copper saddle to bring the cables closer.

especially when the cable is bent into a coil and (2) reduce transient heat generation mechanisms during operation through partial transposition of the HTS tapes, which breaks magnetic flux linkage in the HTS stacks under changing magnetic field conditions [22].

Figure 1 shows a VIPER cable design suitable for DC fusion energy magnets such as the toroidal field (TF) magnet of a tokamak. Superconducting cables in TF magnets typically carry high-currents (I = 25–75 kA) in large magnetic fields (B > 10 tesla), resulting in strong, potentially damaging I×B electromechanical forces that can exceed 1000 kN m^{-1} on the cable. Fusion machine lifetimes require magnets to survive on the order of 10 to 100 thermal cycles and 1000 to 10 000 mechanical load cycles. Cables can range from 100 m to 1000 m in length and require minimum bend radii as low as tens of cm. The tens to hundreds of electrical joints between cables required in a TF magnet must typically be on the order of a few nano-ohms or less per joint for reasonable cryogenic cooling. Thus, TF-suitable cables must provide high-current density, structural strength, and sufficient cooling access in a manufacturable package that can be reliably jointed with nano-ohm resistances.

VIPER cable is based on a specific configuration of the TSTC HTS cable architecture that was first proposed by Takayasu [23] and developed further by Celentano [24]. VIPER cable extends these designs by simplifying the configuration, increasing the current density, and applying a vacuum pressure impregnation (VPI) solder process. A single solder process simultaneously connects the HTS tapes within the cable and joint regions mechanically, electrically, and thermally to each other and to the copper former. There is precedent for soldered superconductors, particularly

early in the development of LTS superconducting technology [25]; however, no cable engineering solution coupling HTS and solder has demonstrated the performance shown in VIPER cable.

Mechanically, soldering converts VIPER cable and joint regions into monolithic structures with no internal component movement. Loads are transferred away from the immobile HTS stacks through the solder and copper former to external structural supports such as stainless-steel jackets or plates [26, 27]. This prevents mechanical degradation from electromagnetic loading and cycling, which has plagued nearly all previous superconducting cables [28, 29].

Electrically, soldering ensures good conductivity among individual HTS tapes in a stack and between HTS stacks and the copper former. This facilitates low-resistance current sharing between the HTS and copper former volumetrically throughout the cable, resulting in uniform current distribution within HTS stacks, good current distribution within joints, and tolerance of HTS quality, manufacturing processes and localized heating. These features relax VIPER manufacturing constraints, allow for lower costs, and increase throughput and reproducibility. Twenty VIPER cables have been produced between 1 and 12 m in length. Cable critical current was consistent and predictable to better than 3% under a variety of operating conditions, including temperature (4.5 K–77 K) and external magnetic field (self-field to 10.9 T), while the fabrication process degraded the cable critical currents from the ideal design value by less than 5%. Post-fabrication CT scans and scanning electron microscope (SEM) imaging of VIPER cables show acceptable solder void sizes under ~3 mm^3 and void fractions under ~5% as seen in figure 4. Importantly, VIPER cable fabrication only requires low temperature processing, close to the melting temperature of solder and does not require any heat treatment processes at high temperatures, a distinct difference to cables using LTS (Nb3Sn) and other HTS (Bi-2212) materials [25, 30].

Thermally, soldering provides a pathway for heat deposited or generated within the HTS stack to move efficiently through the copper former to the central coolant channel. By operating at 20 K, VIPER cables access copper specific heats approximately fifty times larger and thermal conductivities approximately five times larger than LTS cables can at 4 K. The result is high cryostability against the large thermal loads found in many applications, such as nuclear heat loads in fusion or accelerator magnets, AC losses in pulsed magnets, and current-sharing operation in demountable joints and magnets operating with damaged cables.

2.1. Joints

VIPER cable design allows for a simple joint design and manufacturing process. Joints, which supply current to cables, are significant sources of resistive heat load, historically complex, fragile and challenging to fabricate, and often the cause of cable and application failures. The fabrication complexity for joints in LTS cables can be high [30, 31]. While higher temperature stability margins can relax joint resistance requirements in HTS cables, HTS joints to date have not achieved the

simple design, consistent low resistances, and easy fabrication required for commercial applications [16, 32, 33]. Nano-ohm resistances have been achieved, but to do so hundreds of tapes needed to be individually connected per joint, resulting in complex, long, and error-prone fabrication processes that do not scale favorably and make in-field repair and maintenance difficult [34–36].

These challenges are all addressed in VIPER cable. During fabrication, the VPI solder process brings individual HTS tapes into intimate electrical contact with each other, and a roll-formed copper jacket provides a mechanically strong and electrically continuous shell from termination to termination. Thus, the challenge of creating cable joints is reduced to connecting the external copper cable jacket directly to another cable jacket or current lead. As a result, VIPER joints involve minimal manufacturing complexity. For each cable pair, a double saddle is simply clamped between two cable jackets.

An example of a VIPER cable-to-cable joint designed for a cable test in the 'praying-hands' configuration is shown in figure 1. VIPER joints provide a high degree of design flexibility, accommodating, for example, 'shaking hands' style joint configurations and smaller copper saddles. Smaller saddles minimize the distance between cables, reducing joint resistance and increasing current density. Joint fabrication can be completed in several person-hours per joint with basic tooling and produces consistently low resistances. The electrical resistance for four VIPER cable-to-cable joints at operating temperatures and magnetic fields are shown in table 1. These low resistances were maintained over thousands of mechanical loading cycles and multiple thermal cycles. Current was shown to be uniformly distributed within the HTS stack less than 5 cm beyond the joint regions at 77 K, indicating effective current redistribution. The joints were easily disassembled and re-used in a few hours, facilitating access for inspection and maintenance essential in real-world applications. At MIT, a single joint pair was re-used over ten times for cable tests in liquid nitrogen with no change in electrical or mechanical performance. At SULTAN, the joints for the Bravo sample were re-used for the Delta sample and achieved similar (even slightly better) joint resistances as shown in table 1.

3. Cable testing at SULTAN

To assess the mechanical stability, cryostability, and robustness to quench of VIPER cable, four cable pairs—designated Alpha, Bravo, Charlie, and Delta—were tested in the SULTAN facility at the Paul Scherrer Institut [37] under prototypic high-field magnet conditions as shown in figure 2. The primary objective of Alpha, Bravo, and Charlie samples was to maximize the mechanical load achievable per HTS stack—the most important risk for VIPER cables—not the total cable current; the primary objective of the Delta cable was to investigate the effect of multiple stacks per cable and quench detection techniques. HTS with specific performance was chosen to achieve the objectives of each cable test. HTS based on YBCO and GdBCO—with the exact stoichiometry and dopant pinning considered proprietary by the manufacturers—was

Table 1. Summary of VIPER electromechanical tests at SULTAN Results include the electrical resistance in each cable-to-cable joint (at zero magnetic field and average magnetic field to show impact of magnetoresistivity) and degradation of critical temperature (Alpha) and critical current (Bravo, Charlie, Delta) from I×B mechanical cycling and axial strain. HTS with specific critical current performance was selected to achieve the objectives for each test.

| Cable	R_{joint} [nΩ]	I×B cycling carried out at B = 10.9 T and T = 5 K				T_c acquired at B = 10.9 T and I = 7 kA		
		I×B [kN/m] per HTS stack	P_{trans} [MPa] per HTS stack	Axial strain [%]	N_{cycles}	Initial T_c [K]	Final T_c [K]	T_c degradation [%]
Alpha A	2.6 (B_{avg} = 0 T)	185	36	0.0	2000	28.6	27.5	3.8
Alpha B	4.3 (B_{avg} = 3 T)	185	36	0.0	2000	28.0	27.5	2.0
						I_c acquired at B = 10.9 T and T = 10 K		
						Initial I_c [kA]	Final I_c [kA]	I_c degradation [%]
Bravo A	3.2 (B_{avg} = 0 T)	382	75	0.0	1550	29.2	28.1	3.8
Bravo B	5.5 (B_{avg} = 3 T)	382	75	0.0	1550	29.5	28.3	4.1
Charlie A	1.9 (B_{avg} = 0 T)	382	75	0.5	500	29.2	28.2	3.4
Charlie B	1.3 (B_{avg} = 4.3 T)	382	75	0.5	500	29.1	28.2	3.1
Delta A	2.8 (B_{avg} = 0 T)	136	27	0.0	150	45.6	44.5	2.4
Delta B	4.4 (B_{avg} = 3 T)	136	27	0.0	150	43.7	42.6	2.5
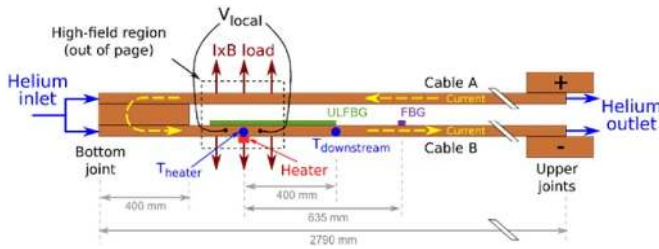
Figure 2. Simplified schematic of VIPER cable test setup at SULTAN. Two VIPER cables are connected by a joint and tested at temperatures between 4.5 K and 20 K and background magnetic fields up to 10.9 T. Instrumentation cited in this paper including voltage taps (V_{local}), temperature sensors (T_{heater}, $T_{downstream}$), fiber optic quench detectors (FBG, ULFBG), and the external heater is shown. I×B loading for mechanical cycling impact on critical current (figure 3) is achieved in the high-field region. Dimensions not to scale.

Figure 3. Critical current degradation over mechanical cycling. I×B mechanical cycling results for the Bravo and Charlie VIPER cable pairs at T = 5 K, and I×B = 382 kN m^{-1}; the critical current was checked at the intervals using voltage tap measurements. Charlie cables had an additional 0.5% axial strain applied. The initial degradation between 3% and 4% consistently stabilizes after 30 cycles. Thermal cycling and current-reversal events occur as indicated with negligible impact on critical current.

intentionally used for different cables to ensure the results were independent of manufacturer, construction, and chemistry.

3.1. Mechanical stability

In high-field magnets, I×B forces can destroy HTS tapes by driving them into surrounding structural material, by creating high tape stack face pressures, and by creating strain from the circumferential expansion of the magnet [38]. The Alpha pair followed the design shown in figure 1 but had one HTS stack each. It underwent 2000 I×B cycles with 17 kA × 10.9 T = 185 kN m^{-1} (36 MPa transverse pressure) on the HTS stack at T = 5 K, a reverse I×B cycle, and a cryogenic-to-room-temperature thermal cycle. Critical temperature (measured at I = 7 kA current and T = 30 K) degraded only slightly (2.0% and 3.8% for the two cables) in the first 30 cycles before stabilizing for the remainder of the test.
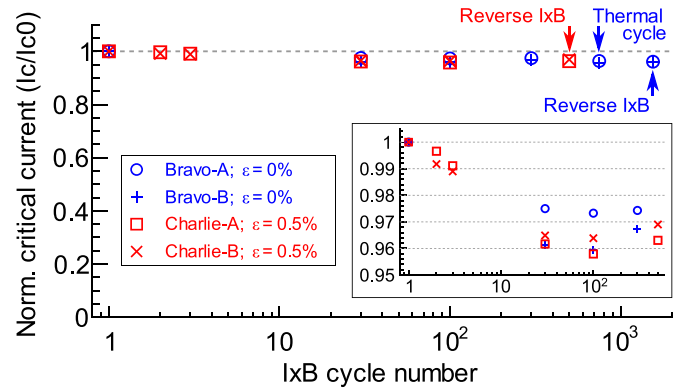
The Bravo and Charlie pairs were identical to each other and had one HTS stack in each cable. They underwent 1550 (Bravo) and 500 (Charlie) I×B cycles at 35 kA × 10.9 T = 382 kN m^{-1} (75 MPa transverse pressure) on the HTS stack at 5 K, a reverse I×B cycle, and a thermal cycle (Bravo). The Charlie cables were axially strained to 0.5% using a specially engineered support structure to simulate the hoop strain that occurs in a magnet. To our knowledge, this is the first simultaneous I×B loading and axial strain test in straight superconducting cables at realistic operating conditions, avoiding the need for placing complex 3D test cables inside expensive and rare large-bore magnets.

The critical current evolution for the Bravo and Charlie pairs are shown in figure 3. Critical current in the four cables degraded by between 3.1% and 4.1% in the first 30 cycles then
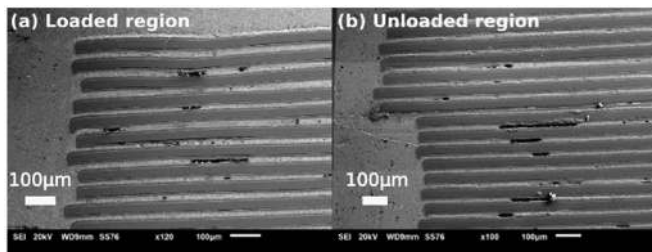
Figure 4. Post-mortem imaging of a VIPER cable. Following tests at SULTAN, one of the cables from the Charlie pair was sectioned, polished, and imaged with a scanning electron microscope to investigate fabrication quality and electromechanical loading on the HTS stack. The region in (a) experienced 500 mechanical cycles at an I×B loading of 382 kN m^{-1} under an axial strain of 0.5% while (b) experienced neither I×B loading or axial strain. Solder uniformity is high with only small, infrequent inter-HTS tape voids. The HTS tape stack and solder show no significant mechanical degradation from load cycling.

stabilized. The ability to withstand 382 kN m^{-1} on a single HTS stack with negligible degradation improves on the previous record of 102 kN m^{-1} by almost a factor of four [11].

The Delta pair (4 HTS stacks each) experienced 150 I×B cycles at 50 kA × 10.9 T = 545 kN m^{-1} for the cable and 136 kN m^{-1} (27 MPa transverse pressure) per HTS stack, two thermal cycles, and 24 quench simulation events. Delta cables responded similarly to cycling as Alpha, Bravo, and Charlie with critical current (I$_c$ = 45.5 kA measured at B = 10.9 T and T = 10 K) degradations of 2.4% and 2.5%.

A summary of the electromechanical results is shown in table 1. For all eight cables, performance degradation asymptoted to between 2.0% and 4.1%, independent of cable fabrication specifics, HTS tape manufacturer, I×B loading, axial strain, and operating conditions. Sectioning, polishing, and SEM imaging of the cables after the SULTAN tests, such as a cable from the Charlie pair shown in figure 4, showed no significant macroscopic mechanical damage due to the immobilization of the HTS tapes in the solder.

Microscopic 100 μm lengths of REBCO layers were observed in inter-HTS tape solder voids, and had separated from their substrates. These low-density microscopic defects—due to a combination of fabrication imperfections and mechanical cycling—do not significantly degrade the electrical performance. Electromechanical finite element analysis was performed and suggests that plastic strains in the solder, which concentrate at the corner tips of the HTS stack and approach 1%, likely cause a few percent of the HTS tape to degrade under loading, consistent with experimental observations. The analysis showed that ensuring good HTS structural support through good solder ductility, small solder coefficient of thermal expansion, and strong solder adhesion to the HTS and copper former are the key drivers to eliminate critical current degradation.

The immobilization of the HTS stacks provided by the VPI solder mitigates I$_c$ degradation from large I×B forces in VIPER cables and effectively transfers the force into the surrounding steel support structure. Because of the cable twist pitch, I×B forces applied during SULTAN testing were incident not just normal to the flat of the tape (favorable direction) but in the shear direction (unfavorable direction) as well. No significant delamination of HTS was observed in SEM imaging of cable anywhere along the twist pitch, corroborating the absence of I$_c$ and joint resistance degradation despite up to 2000 I×B cycles in SULTAN tests. This compares favorably to the challenging development of LTS Nb$_3$Sn cables for fusion magnets, in which substantial efforts were required to overcome the large and continuous I$_c$ degradation observed in SULTAN tests [39], and to other present HTS cable concepts, in which repeated movement of HTS stacks or sub-strands caused unstabilized I$_c$ degradation of 10% to 20% at 2000 cycles under twelve times less I×B force (~30 kN m^{-1}) and seven times less transverse pressure (~10 MPa) per HTS stack than was applied to VIPER cables [40]. Because force per stack—not total cable current—is the critical risk retirement metric for eliminating I$_c$ degradation, a VIPER cable with six HTS stacks with roughly six times the current density of the Bravo or Charlie cables can be deployed with minimal additional risk of I$_c$ degradation.

3.2. Cryostability & quench

Off-normal heating in a superconducting cable can cause thermal runaway known as quench, which has been a major outstanding issue for insulated HTS magnets, particularly for fusion and accelerator magnets with large stored energy. Quench detection in HTS cables is more challenging than in LTS cables due to their higher thermal stability, which can cause lower normal zone propagation velocities (NZPVs), slower detection times, and higher probability of damage [41, 42]. Quench detection techniques that are fast enough to avoid damage in practical HTS cable-based magnets with high electrical noise and significant energy storage have not been demonstrated to date.

For the Delta cables in SULTAN, NZPVs were measured by using the propagation of a 100 μV cm^{-1} electric field front on axial voltage tap arrays during quench events with results between 0.04 and 0.42 m s^{-1} under various operating conditions (B = 10.9 T; T = 10 K, 20 K; operating current I$_{op}$ = 36.0 kA, 40.5 kA, 45.0 kA, 47.5 kA; I$_{op}$/I$_c$ = 0.8, 0.9, 1.0, 1.05). The measured NZPVs were equal to or faster than those measured in individual HTS tapes, which have been found between 0.07 and 0.13 m s^{-1} for typical operating conditions [41]. VIPER NZPVs approach those in LTS conductors [43], are consistent with analytical calculations [44], and enable a wide optimization for voltage tap-based quench detection systems on VIPER cables.

Figure 5 shows a Delta cable recovering from three increasing-duration 45 W external resistive heater pulses but quenching on a fourth. A detailed multiphysics model successfully captures the superconducting, electrical, thermal, and magnetic behavior of the cables without relying on any free parameters. Figure 6 shows a model-generated cryostability map with a predictive boundary between stability and quench in response to external heating that is in good agreement with
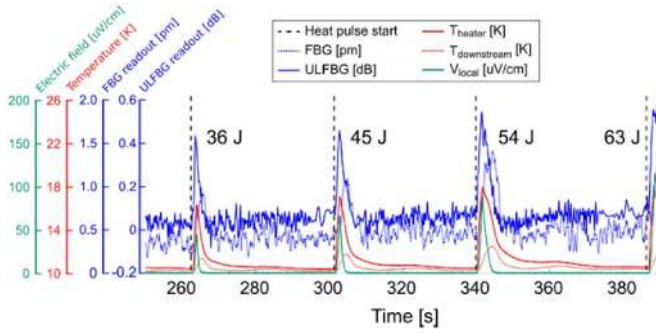
Figure 5. Heat pulse response and quench detection. Four external heater pulses at 45 W depositing energies of 36 J, 45 J, 54 J, and 63 J into a Delta cable operated at B = 10.9 T, T = 10 K, I_{op}/I_c = 0.9, and m_{He} = 2.0 g s^{-1}. The cable returns to stable operation after the first three pulses despite current sharing with local electric fields reaching 85 μV cm^{-1}. The cable quenches after the fourth pulse. Two fiber optic quench detection technologies, based on FBG and ULFBG techniques, track temperature excursions with local temperature sensitivities of 1–2 K and with ULFBG detection times approaching 5 ms.
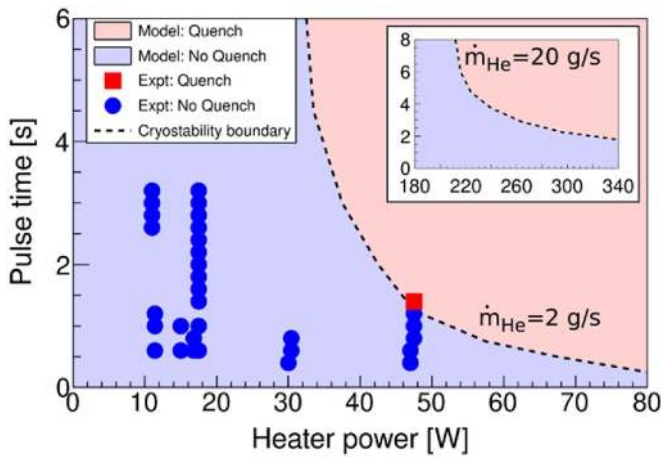

Figure 6. VIPER cable cryostability map. A multiphysics model predicting the cryostability boundary in response to external heater pulses of increasing power and time for conditions B = 10.9 T, T = 10 K, I_{op}/I_c = 0.9, and $\dot{m}_{He}$ = 2.0 g s^{-1}. The available experimental data in these conditions shows good agreement with the model. The inset shows the enhanced cryostability that is achievable in VIPER cable applications with increase helium mass flow rate.

measured data. The model confirms that VIPER cryostability results from the favorable combination of high heat capacity and low electrical resistance of the copper former at 20 K, the amount of copper used, and the rapid heat removal pathway provided by the VPI soldering of the HTS and copper former.

At typical cable operating conditions (B = 10.9 T, T = 20 K, I_c = 31.5 kA, I_{op} < 31.5 kA, I_{op}/I_c < 1.0, and helium mass flow rate $\dot{m}_{HE}\dot{m}$ = 2.0 g s^{-1}), Delta cables were stable up to 0.8 MW m^{-3} of heating, induced by the external heater running at 57 W for up to 15 s and depositing 0.9 kJ of energy. In response to heater pulses greater than 47 W, the cables recovered from strong current-sharing operation with electric fields in excess of 100 μV cm^{-1}, 100 times greater

than the 1 μV cm^{-1} HTS superconducting-to-normal transition criterion. Quenches in response to external heater pulses were almost exclusively observed at T < 20 K and I_{op}/I_c > 1.0.

Temperature excursions on the Delta cable were monitored with two fiber optic quench detection technologies: an array of discrete fiber Bragg gratings (FBG) [45] and a distributed single ultra-long FBG (ULFBG) [46]. Each technique uses a variation of monitoring the temperature-dependent spectral response of FBG inscribed into optical fibers. FBG and ULFBG coated optical fibers were embedded in the outer circumference of the Delta cable copper jackets, ensuring good thermal contact and mechanical protection. Figure 5 shows that both technologies demonstrated consistent, unambiguous detection of local temperature excursions of 2 K to 3 K. ULFBG detection times were on the order of 100 ms, oven ten times shorter than time-to-damage from quenches in superconducting fusion magnets [47]. FBG response times to hot spots at the gratings are as rapid but total detection times are dependent on the grating spacing and NZPV.

Both techniques represent improvement over traditional voltage tap approaches in, for example, large-scale fusion magnets, which require multi-second wait times to achieve sufficient signal-to-noise and could result in potentially destructive temperature rises up to 150 K [48]. The two fiber-optic systems are complementary: the ULFBG system is a sectional measurement that provides fast detection times at the expense of positional information; the FBG system provides spatially resolved temperature excursions anywhere in the cable but requires time for the normal zone to propagate to the nearest discrete grating. Both technologies have favorable scaling to the 100 m lengths required for high-field fusion magnets and other applications, requiring manufacturing of longer fibers but utilizing the same equipment and analysis techniques used in the shorter experiments described here.

4. Discussion

VIPER cable demonstrates high mechanical strength, high cryostability, and rapid quench detection. Its performance is predictable and repeatable, allowing for high-confidence design. Its manufacturing process is simple and scalable to long lengths, and its simple, demountable joints allow for the repairability, access, maintenance and inspectability required by real-world applications. VIPER cable expands the performance boundaries of many critical energy generation and transmission technologies. It will, for example, enable the performance of large-scale high-field superconducting magnets to push well past 15 T. Such high-field superconducting magnet technology is presently enabling the high magnetic field pathway to accelerated fusion energy [49, 50], including in the SPARC tokamak, an experiment seeking the demonstration of net fusion energy by the mid 2020's, and slated to begin construction in 2021 [51]. VIPER cable may also be relevant to high-energy physics detector magnets like those planned for the future circular collider [52]. And it may find use in DC power cables, in the DC field winding components of electric motors and generators in the 10+ MW class, as well as in

magnetic energy storage devices. This note has focused on the DC application of VIPER cable; however, AC applications are foreseen, and AC loss measurements were performed as part of the SULTAN tests. The results of these measurements and impact on VIPER cable suitability for AC applications will be reported in full in a future publication. Combined, these application categories are expected to drive significant scale up of HTS industry volumes and a corresponding reduction in cost. HTS demand in excess of 1000 km yr^{-1} is projected to drive the price of HTS tape below the \$50/kA-m level over the next decade, greatly accelerating wide-scale application [20, 21]. We expect cost-effective VIPER cables to replace LTS cable in present and future applications and open new opportunities previously inaccessible to superconducting technology.

Acknowledgments

ORCID iDs

Brandon N Sorbom ⊙ https://orcid.org/0000-0002-2110-6766
Rodney A Badcock ⊙ https://orcid.org/0000-0003-0219-9570

References

[1] Onnes H K 1912 Further experiments with liquid helium G. On the electrical resistance of pure metals etc. VI. On the sudden change in the rate at which the resistance of mercury disappears *KNAW Proc.* **14** 818–21

[2] Kunzler J E, Buehler E, Hsu F S L and Wernick J H 1961 Superconductivity in Nb$_3$Sn at high current density in a magnetic field of 88 kgauss *Phys. Rev. Lett.* **6** 89–91

[3] Bednorz J G and Muller K A 1986 Possible highT c superconductivity in the Ba-La-Cu-O system *Z. Phys.* B **64** 189–93

[4] Goyal A *et al* 1996 High critical current density superconducting tapes by epitaxial deposition of YBa2Cu3Ox thick films on biaxially textured metals *Appl. Phys. Lett.* **69** 1795–7

[5] Usoskin A, Freyhardt H C, Issaev A, Dzick J, Knoke J, Oomen M P, Leghissa M and Neumueller H-W 2003 Large area YBCO-coated stainless steel tapes with high critical currents *IEEE Trans. Appl. Supercond.* **13** 2452–7

[6] Markiewicz W D *et al* 2012 Design of a superconducting 32 T magnet with REBCO high field coils *IEEE Trans. Appl. Supercond.* **22** 4300704–4300704

[7] Maeda H, Shimoyama J, Yanagisawa Y, Ishii Y and Tomita M 2019 The MIRAI program and the new super-high field NMR initiative and its relevance to the development of superconducting joints in Japan *IEEE Trans. Appl. Supercond.* **29** 1–9

[8] Takayasu M, Chiesa L, Bromberg L and Minervini J V 2011 Cabling method for high current conductors made of HTS tapes *IEEE Trans. Appl. Supercond.* **21** 2340–4

[9] Laan D C V D 2009 YBa2Cu3O7-δcoated conductor cabling for low ac-loss and high-field magnet applications *Supercond. Sci. Technol.* **22** 065013

[10] Goldacker W, Grilli F, Pardo E, Kario A, Schlachter S I and Vojenčiak M 2014 Roebel cables from REBCO coated conductors: a one-century-old concept for the superconductivity of the future *Supercond. Sci. Technol.* **27** 093001

[11] Takayasu M, Chiesa L, Noyes P D and Minervini J V 2017 Investigation of HTS twisted stacked-tape cable (TSTC) conductor for high-field, high-current fusion magnets *IEEE Trans. Appl. Supercond.* **27** 1–5

[12] Uglietti D, Sedlak K, Wesche R, Bruzzone P, Muzzi L and Della Corte A 2018 Progressing in cable-in-conduit for fusion magnets: from ITER to low cost, high performance DEMO *Supercond. Sci. Technol.* **31** 055004

[13] Bykovsky N, Uglietti D, Wesche R and Bruzzone P 2018 Damage investigations in the HTS cable prototype after the cycling test in EDIPO *IEEE Trans. Appl. Supercond.* **28** 1–5

[14] Celentano G, Vannozzi A, De Marzi G, Marchetti M, Augieri A, Di Zenobio A, Fabbri F, Muzzi L, Rufoloni A and Della Corte A 2019 Bending behavior of HTS stacked tapes in a cable-in-conduit conductor with twisted Al-slotted core *IEEE Trans. Appl. Supercond.* **29** 1–5

[15] Wolf M J, Bagrets N, Fietz W H, Lange C and Weiss K-P 2018 Critical current densities of 482 A/mm2 in HTS CrossConductors at 4.2 K and 12 T *IEEE Trans. Appl. Supercond.* **28** 1–4

[16] Laan D C V D, Weiss J D and McRae D M 2019 Status of CORC® cables and wires for use in high-field magnets and power systems a decade after their introduction *Supercond. Sci. Technol.* **32** 033001

[17] Uglietti D 2019 A review of commercial high temperature superconducting materials for large magnets: from wires and tapes to cables and conductors *Supercond. Sci. Technol.* **32** 053001

[18] Laan D C V D *et al* 2020 A CORC® cable insert solenoid: the first high-temperature superconducting insert magnet tested at currents exceeding 4 kA in 14 T background magnetic field *Supercond. Sci. Technol.* **33** 05LT03

[19] Whyte D G *et al* 2016 *Smaller & Sooner: Exploiting High Magnetic Fields from New Superconductors for a More Attractive Fusion Energy Development Path* (New York: Springer US)

[20] Matias V and Hammond R H 2012 YBCO superconductor wire based on IBAD-textured templates and RCE of YBCO: process economics *Phys. Procedia* **36** 1440–4

[21] Grant P M 1997 Superconductivity and electric power: promises, promises … past, present and future *IEEE Trans. Appl. Supercond.* **7** 112–33

[22] Dahl P F, Morgan G H and Sampson W B 1969 Loss measurements on twisted multifilamentary superconducting wires *J. Phys. D: Appl. Phys.* **40** 2083–5

[23] Takayasu M, Minervini J V and Bromberg L 2013 Superconductor cable

[24] Celentano G, De Marzi G, Fabbri F, Muzzi L, Tomassetti G, Anemona A, Chiarelli S, Seri M, Bragagni A and Della

Corte A 2014 Design of an industrially feasible twisted-stack HTS cable-in-conduit conductor for fusion application *IEEE Trans. Appl. Supercond.* **24** 1–5

[25] Bruzzone P 1999 Superconductors, forced flow conductor manufacturing *Wiley Encyclopedia of Electrical and Electronics Engineering* (New York: American Cancer Society)

[26] Hoenig M and Montgomery D 1975 Dense supercritical-helium cooled superconductors for large high field stabilized magnets *IEEE Trans. Magn.* **11** 569–72

[27] Huguet M, Team I J C and Teams I H 2001 Key engineering features of the ITER-FEAT magnet system and implications for the R&D programme *Nucl. Fusion* **41** 1503–13

[28] Mitchell N, Devred A, Larbalestier D C, Lee P J, Sanabria C and Nijhuis A 2013 Reversible and irreversible mechanical effects in real cable-in-conduit conductors *Supercond. Sci. Technol.* **26** 114004

[29] Sanabria C, Lee P J, Starch W, Devred A and Larbalestier D C 2015 Metallographic autopsies of full-scale ITER prototype cable-in-conduit conductors after full cyclic testing in SULTAN: II. Significant reduction of strand movement and strand damage in short twist pitch CICCs *Supercond. Sci. Technol.* **28** 125003

[30] D'Auria V, Stepanov B, Sedlak K and Bruzzone P 2020 Inter-layer joint of Nb3Sn react wind cables for fusion magnets *IEEE Trans. Appl. Supercond.* **30** 1–5

[31] Stepanov B, Bruzzone P and Sedlak K 2018 Inter-layer joint for the TF coils of DEMO—design and test results *IEEE Trans. Appl. Supercond.* **28** 1–4

[32] Takayasu M, Chiesa L and Minervini J V 2014 Development of termination methods for 2G HTS tape cable conductors *IEEE Trans. Appl. Supercond.* **24** 1–5

[33] Nishio T, Ito S and Hashizume H 2017 Heating and loading process improvement for indium inserted mechanical lap joint of REBCO tapes *IEEE Trans. Appl. Supercond.* **27** 1–5

[34] Mulder T 2018 *Advancing ReBCO-CORC Wire and Cable-in-conduit Conductor Technology for Superconducting Magnets* (Enschede, Netherlands: University of Twente)

[35] Ito S, Hashizume H, Yanagi N and Tamura H 2019 Bridge-type mechanical lap joint of HTS STARS conductors using an integrated joint piece *Fusion Eng. Des.* **146** 590–3

[36] Uglietti D, Bykovsky N, Sedlak K, Stepanov B, Wesche R and Bruzzone P 2015 Test of 60 kA coated conductor cable prototypes for fusion magnets *Supercond. Sci. Technol.* **28** 124005

[37] Stepanov B, Bruzzone P, Sedlak K and Croari G 2013 SULTAN test facility: summary of recent results *Fusion Eng. Des.* **88** 282–5

[38] Pierro F, Zhao Z, Chiesa L and Takayasu M 2017 Finite element investigation of the mechanical behaviour of a twisted stacked-tape cable exposed to large Lorentz loads *IOP Conf. Ser.: Mater. Sci. Eng.* **279** 012035

[39] Devred A, Backbier I, Bessette D, Bevillard G, Gardner M, Jong C, Lillaz F, Mitchell N, Romano G and Vostner A 2014 Challenges and status of ITER conductor production *Supercond. Sci. Technol.* **27** 044001

[40] Bykovsky N, Uglietti D, Sedlak K, Stepanov B, Wesche R and Bruzzone P 2016 Performance evolution of 60 kA HTS cable prototypes in the EDIPO test facility *Supercond. Sci. Technol.* **29** 084002

[41] van Nugteren J, Dhallé M, Wessel S, Krooshoop E, Nijhuis A and Ten Kate H 2015 Measurement and analysis of normal zone propagation in a ReBCO coated conductor at temperatures below 50K *Phys. Procedia* **67** 945–51

[42] Kang R *et al* 2020 Quench simulation of REBCO cable-in-conduit conductor with twisted stacked-tape cable *IEEE Trans. Appl. Supercond.* **30** 1–7

[43] Zanino R, Bonifetto R, Brighenti A, Isono T, Ozeki H and Savoldi L 2018 Prediction, experimental results and analysis of the ITER TF insert coil quench propagation tests, using the 4C code *Supercond. Sci. Technol.* **31** 035004

[44] Iwasa Y 2009 *Case Studies in Superconducting Magnets: Design and Operational Issues* (New York: Springer US)

[45] Chiuchiolo A, Bajas H, Bajko M, Bottura L, Consales M, Cusano A, Giordano M and Perez J C 2016 Advances in fiber optic sensors technology development for temperature and strain measurements in superconducting magnets and devices *IEEE Trans. Appl. Supercond.* **26** 1–5

[46] Badcock R A and Fisser M Optical Fibre Sensing System and Method

[47] Coatanea-Gouachet M, Carrillo D, Lee S and Rodríguez-Mateos F 2015 Electromagnetic quench detection in ITER superconducting magnet systems *IEEE Trans. Appl. Supercond.* **25** 1–7

[48] Martovetsky N N and Radovinsky A L 2014 ITER CS quench detection system and its qualification by numerical modeling *IEEE Trans. Appl. Supercond.* **24** 1–4

[49] Whyte D 2019 Small, modular and economically attractive fusion enabled by high temperature superconductors *Phil. Trans. R. Soc.* A **377** 20180354

[50] Authors T B D 2020 High-field fusion roadmap article title TBD *Supercond. Sci. Technol.* In preparation

[51] Creely A J 2020 *et al* Overview of the SPARC Tokamak *JPP* 9

[52] Mentink M *et al* 2018 Evolution of the conceptual FCC-hh baseline detector magnet design *IEEE Trans. Appl. Supercond.* **28** 1–10